

Hole spectral functions in lightly doped quantum antiferromagnets

Satyaki Kar⁽¹⁾ and Efstratios Manousakis^(1,2)

¹*Department of Physics, Florida State University, Tallahassee, FL 32306-4350, USA and*

²*Department of Physics, University of Athens, Panepistimioupolis, Zografos, 157 84 Athens, Greece.*

(Dated: October 24, 2018)

We study the hole and magnon spectral functions as a function of hole doping in the two-dimensional (2D) $t - J$ and $t - t' - t'' - J$ models working within the limits of the spin-wave theory, by linearizing the hole-spin-deviation interaction and by adapting the non-crossing approximation (NCA). We find that the staggered magnetization decreases rather rapidly with doping and it goes to zero at a few percent of hole concentration in both $t - J$ and the $t - t' - t'' - J$ model. We find that with doping, the residue of the quasiparticle peak at $\vec{G} = (\pm\pi/2, \pm\pi/2)$ decreases rapidly with doping and the spectral function is in agreement with high resolution angle-resolved photo-emission spectroscopy (ARPES) studies of the copper-oxide superconductors. The observed large shift of the chemical potential inside the Mott gap is found to be a result of broadening of the quasiparticle peak. We find pockets centered at \vec{G} , similar to those observed by quantum oscillation measurements, (i) with an elliptical shape with large eccentricity along the anti-nodal direction in the case of the $t - J$ model, and (ii) with an almost circular shape in the case of the $t - t' - t'' - J$ model. We also find that the spectral intensity distribution in the doped antiferromagnet has a waterfall-like pattern along the nodal direction of the Brillouin zone, a feature that is also seen in ARPES measurements.

PACS numbers: 71.10.-w, 71.10.Fd, 71.27.+a, 74.72.-h, 79.60.-i

I. INTRODUCTION

During the last two decades there is significant progress in angle-resolved photo-emission spectroscopy (ARPES) due to improved energy and angle resolution by at least an order of magnitude¹⁻⁹. Furthermore, advances in improving sample quality and characterization have enabled ARPES to become a leading tool in the investigation of otherwise hidden information about copper-oxide based superconducting (COSC) materials. ARPES directly exposes the momentum and frequency dependent imaginary part of the single particle Green's function, a quantity which sits at the heart of quantum many-body theory.

As the wave-number of the incident photon is varied, a smooth transition of the intensity resembling a waterfall-like pattern is observed in ARPES of the COSC materials at various hole or electron doping concentrations^{3-6,8}. While it has been argued that this could be a matrix element effect¹⁰, similar intensity features are obtained by means of theoretical models and recently in different materials and under various conditions⁹. Quantum Monte Carlo calculations showed such intensity pattern in 2D Hubbard models¹¹. In addition, it was suggested¹² that these waterfall-like features of the ARPES intensity are caused by the gradual transfer of the spectral weight from the lowest energy quasiparticle peak at the wavevector $\vec{G} = (\pm\pi/2, \pm\pi/2)$ to the higher energy so-called "string" states as the incident wave-vector gradually moves towards $(0, 0)$ along the nodal direction of the Brillouin zone. This suggestion was based on a calculation of the single hole spectral function in the $t - J$ model by *broadening* the peaks of the spectral function corresponding to the string excitations¹². Later, the broad-

ening required to achieve a reasonable agreement with the APRES spectra was obtained by considering the effects of optical phonons at finite temperatures¹³. In the present paper we use the $t - J$ and $t - t' - t'' - J$ models within the limits of the spin-wave theory by linearizing the hole-spin-deviation interaction and within the non-crossing approximation (NCA) to study the effects of doping on the single-hole spectral functions. We show that the *broadening* of the peaks corresponding to the high energy string excitations can be achieved naturally as an effect of doping, thus, leading to a smooth waterfall-like intensity distribution along the nodal direction of the Brillouin zone.

Sometime ago, ARPES studies¹⁴ on the undoped parent COSC compounds reveal the existence of a relatively well-defined low-energy quasiparticle peak at wavevector \vec{G} which follows a dispersion with a bandwidth of similar magnitude to that calculated in Ref. 36. Rather recently, however, Fournier et al.⁹, reported that the quasiparticle residue as a function of doping is essentially zero below approximately 10% hole concentration. In addition, Shen et al.¹⁵ have reported ARPES measurements where the quasiparticle peak has a broad line shape (much broader than the ARPES resolution) and they also found what they call a "paradoxical shift" of the chemical potential within the Mott gap. Our results indicate that these seemingly contradictory findings can be reconciled using the calculations reported in the present paper. We find that the lowest energy quasiparticle peak observed near $(\pm\pi/2, \pm\pi/2)$ in the undoped cuprates¹⁴, is very sensitive to a small amount of doping. Namely, the quasiparticle residue rapidly goes to zero as a function of doping concentration, and, in addition, it is known that optical phonons broaden the peak¹³. Furthermore, we find that the facts, that the quasiparticle peak is broad and that

the chemical potential is shifted relative to the quasiparticle peak position, are not two independent effects. When we repeated our calculation by broadening the quasiparticle peak we found that the broadening itself leads to a very significant shift of the chemical potential relative to the lowest energy quasiparticle position which can be understood in a straightforward manner.

Furthermore, we find that, at low doping, elliptical hole pockets form, which are centered around \vec{G} , in agreement with rather recent quantum oscillation measurements³⁸. Our calculated intensity of the spectral function shows that there are luminous elliptical rings centered around the points \vec{G} of the Brillouin zone. We argue that these rings could be related to the banana-like features seen in ARPES reported on the under-doped COSC materials². Our formulation, which is based on the existence of antiferromagnetic (AF) long-range-order (LRO), cannot yield a spectrum sharing the single-banana-like feature seen in ARPES, where only one side around the \vec{G} is luminous. The reason lies in the reflection symmetry about the line $(\pi, 0) \rightarrow (0, \pi)$ of the Brillouin zone which is present when AF-LRO is present in the system. Therefore, we view the banana-like shape as a result produced by “scissoring” the elliptical ring along the above symmetry line, an operation which breaks this symmetry required by the AF-LRO. The measurements presented in Ref. 2 were carried out in materials which lack AF-LRO.

Linear spin-wave (LSW) theory can describe the undoped and lightly doped antiferromagnets as long as AF-LRO is present in the system. In the undoped COSC parent compounds, which are antiferromagnetic insulators⁴¹, the AF-LRO disappears at a very low doping concentration. For example, in $La_{2-x}Sr_xCuO_4$, the AF-LRO is destroyed at doping $x \sim 0.015$ ¹⁸. On the other hand, magnetic fluctuations persist even at higher doping concentrations and short-range spin correlations are observed in the inelastic neutron scattering experiments at reasonably high doping concentrations¹⁸⁻²⁰. Calculations on $t-J$ and related models also show the staggered magnetization of the system to go to zero as the undoped system is gradually doped with holes²¹⁻²⁵.

In order to study the 2D hole-doped antiferromagnet, we have considered the $t-J$ and $t-t'-t''-J$ models working within the limits of the spin-wave theory, by linearizing the hole-spin-deviation interaction and by adapting the NCA. Within the NCA the self-energy diagrams are considered for both holes and magnons and the Dyson’s equation is solved to obtain the one-particle Green’s function. The contribution of the magnon polarization bubbles are considered and, thus, the magnon-mediated hole-hole interaction is included. We should mention here that we do not use the rigid band approximation which uses the hole bands of the single hole calculation to obtain the hole spectra at finite concentration neither do we use any approximate form of the hole spectral function to write it as a sum of a coherent quasiparticle peak and an incoherent continuum^{16,17}.

Hole and magnon Green’s functions for a 2D $t-J$

model at finite-doping, using LSW approximation and NCA, have been studied earlier (Ref. 27). However, the goal and focus of the present study is quite different; as already discussed, there are rather recent high resolution ARPES studies which exhibit the existence of the waterfall features^{3-6,8} and other studies which reveal the shape of the most intense part of the Brillouin zone near the Fermi surface^{2,9}. Our calculations are done with the aim to understand, if possible, these and related features of the ARPES measurements. In addition, as we will discuss in the paper, our results differ significantly from the results of Ref. 27. For example, we find that only a few percent hole concentration is enough to destroy the long-range antiferromagnetic order, while in Ref. 27 results for the spectral function were presented for up to hole doping $x \sim 0.25$, where we find that this approach breaks down precisely because there is no LRO for this level of doping.

Our approach discussed above relies on the existence of AF-LRO both within the model and in the materials which we plan to apply our findings, therefore, we only hope to capture the physics of the real materials in the limit of light doping. It is known, however, that even in the above models the AF-LRO may be unstable upon doping leading to other forms of order, such as spiral order^{16,28,29}, stripe ordering^{30,31} or phase separation instability^{32,33}. Therefore, we begin by assuming that the AF-LRO is present in the system at low doping and we proceed with a perturbative approach which asserts that spin wave excitations are well-defined in the system. If the AF order ceases to exist and it gets replaced by any of the above phases, this should show up as an instability in our calculation. We will discuss this further in Sec. IV.

The paper is organized as follows: In the next section we discuss the formulation and the approximation scheme followed in this work. In Sec. A of the Appendix we outline some of the technical details of the calculation. In Sec. III we present our results on the hole spectral functions, the hole energy momentum dispersions and the intensity of the spectral functions is compared with the waterfall and banana-like features observed in ARPES. In Sec. IV A our results on the magnon spectral functions, the magnon dispersion relations, and the staggered magnetization as a function of doping are presented. In Sec. V we summarize our findings and conclusions.

II. FORMULATION

The 2D $t-J$ or the $t-t'-t''-J$ model, when expressed in terms of operators which create spin-deviations above the Néel order and by keeping up to quadratic terms in these operators, can be approximated by the following

Hamiltonian³⁶

$$\begin{aligned}
H = & E_0 + \sum_{\mathbf{k}} \epsilon_k (f_{\mathbf{k}}^\dagger f_{\mathbf{k}} + h_{\mathbf{k}}^\dagger h_{\mathbf{k}}) + \sum_{\mathbf{k}} \Omega_{\mathbf{k}} (\alpha_{\mathbf{k}}^\dagger \alpha_{\mathbf{k}} + \beta_{\mathbf{k}}^\dagger \beta_{\mathbf{k}}) \\
& + \sum_{\mathbf{k}, \mathbf{q}} h_{\mathbf{k}}^\dagger f_{\mathbf{k}-\mathbf{q}} [g(\mathbf{k}, \mathbf{q}) \alpha_{\mathbf{q}} + g(\mathbf{k}-\mathbf{q}, -\mathbf{q}) \beta_{-\mathbf{q}}^\dagger] \\
& + f_{\mathbf{k}}^\dagger h_{\mathbf{k}-\mathbf{q}} [g(\mathbf{k}-\mathbf{q}, -\mathbf{q}) \alpha_{-\mathbf{q}}^\dagger + g(\mathbf{k}, \mathbf{q}) \beta_{\mathbf{q}}] + H.c. \quad (1)
\end{aligned}$$

where $h_{\mathbf{k}}, f_{\mathbf{k}}$ are the spin-less hole annihilation operators (the so-called slave fermions) for \downarrow and \uparrow sub-lattices respectively and $\alpha_{\mathbf{k}}, \beta_{\mathbf{k}}$ are the magnon annihilation operators for the corresponding sub-lattices. ϵ_k, Ω_k are bare hole and magnon energies respectively with $\epsilon_k = 0$ for $t - J$ model and $\epsilon_k = 4t' \cos k_x \cos k_y + 2t'' [\cos 2k_x + \cos 2k_y]$ for $t - t' - t'' - J$ model. We use the parameters $t' = -0.33t$ and $t'' = 0.22t$ that gives good fit with ARPES results of the energy band along anti-nodal directions³⁵. The coupling constants $g(\mathbf{k}, \mathbf{q})$ are defined in Ref. 36.

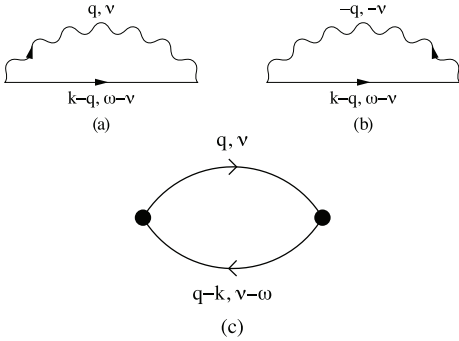


FIG. 1: NCA self-energy diagrams for holes (a,b) and magnons (c).

For a system doped with holes, the Dyson's equations for hole/spin-wave excitations become

$$\begin{aligned}
G(\mathbf{k}, \omega) &= \frac{1}{\omega - \epsilon_{\mathbf{k}} - \Sigma(\mathbf{k}, \omega) + i \operatorname{sgn}(\omega - \mu)\eta}, \\
D(\mathbf{k}, \omega) &= \frac{1}{\omega - \Omega_{\mathbf{k}} - \Pi(\mathbf{k}, \omega) + i\eta}, \quad (2)
\end{aligned}$$

where $G(\mathbf{k}, \omega)$ and $D(\mathbf{k}, \omega)$ are the hole and magnon Green's functions and $\Sigma(\mathbf{k}, \omega)$ and $\Pi(\mathbf{k}, \omega)$ are the respective self-energies. μ is the chemical potential for holes and η is the broadening parameter. Here we would like to note that for a doping concentration of x in a system of total number of sites N , the single-hole Green's function describes the spectral properties of a hole (or rather a fermionic excitation) added or removed from the system where xN number of holes are already present.

In this paper we will work within the so-called non-crossing approximation (NCA), as the higher order vertex corrections have been shown earlier to be small^{36,37}.

The NCA self-energies are given by

$$\begin{aligned}
\Sigma(\mathbf{k}, \omega) &= \frac{i}{2\pi} \sum_{\mathbf{q}} \int d\nu [g^2(\mathbf{k}, \mathbf{q}) G(\mathbf{k}-\mathbf{q}, \omega-\nu) D(\mathbf{q}, \nu) \\
&\quad + g^2(\mathbf{k}-\mathbf{q}, -\mathbf{q}) G(\mathbf{k}-\mathbf{q}, \omega-\nu) D(-\mathbf{q}, -\nu)], \\
\Pi(\mathbf{k}, \omega) &= -\frac{i}{2\pi} \sum_{\mathbf{q}} g^2(\mathbf{q}, \mathbf{k}) \int d\nu G(\mathbf{q}-\mathbf{k}, \nu-\omega) G(\mathbf{q}, \nu). \quad (3)
\end{aligned}$$

The two terms of the hole self-energy describe the hole motion outside the Fermi-sea (of holes) and electron motion inside the Fermi-sea respectively. Fig 1(a) describes hole motion forward in time where as Fig 1(b) describes hole motion backward in time which is equivalent to electron motion forward in time. It can be easily shown that this second term becomes zero for an undoped system.

Fig 1(c) shows the magnon self-energy or spin-polarization bubble. This term is also non-zero only for the system with finite doping.

We can get rid of the infinite limits of the energy integral over ν if we utilize the spectral representations of the Green's functions:

$$\begin{aligned}
\mathcal{G}(\mathbf{k}, \omega) &= \int_{-\infty}^{\infty} d\epsilon \left[\frac{A(\mathbf{k}, \epsilon)}{\omega - \epsilon - \mu + i\eta} + \frac{B(\mathbf{k}, \epsilon)}{\omega - \epsilon - \mu - i\eta} \right] \quad (4) \\
D(\mathbf{k}, \omega) &= \int_{-\infty}^{\infty} \frac{C(\mathbf{k}, \epsilon) d\epsilon}{\omega - \epsilon + i\eta}, \quad (5)
\end{aligned}$$

where μ is Fermi energy and $A(\mathbf{k}, \epsilon), B(\mathbf{k}, \epsilon)$ are hole spectral functions defined as

$$\begin{aligned}
A(k, \omega) &= \sum_n |\langle n | h_k^\dagger | \psi \rangle|^2 \delta(\omega - \epsilon_n^{N+1}), \\
B(k, \omega) &= \sum_m |\langle m | h_k | \psi \rangle|^2 \delta(\omega + \epsilon_m^{N-1}), \quad (6)
\end{aligned}$$

where $\{|n\rangle\}$ and $\{|m\rangle\}$ denote the complete set of basis states for $(N+1)$ and $(N-1)$ hole/particle systems and ϵ_n^{N+1} and ϵ_m^{N-1} are the corresponding energies. Here $|\psi\rangle$ is the interacting ground state of the Hamiltonian. $C(\mathbf{k}, \epsilon)$ is the magnon spectral function defined as

$$C(k, \omega) = \sum_n |\langle n | \alpha_k^\dagger | \psi \rangle|^2 \delta(\omega - \omega_n), \quad (7)$$

where ω_n is the energy of the state $|n\rangle$ which can be connected to the ground state via the magnon creation operator.

Using these auxiliary functions, the imaginary part of the self-energy takes the following form

$$\begin{aligned}
\Sigma_I(\mathbf{k}, \omega) &= -\frac{1}{\pi} \sum_{\mathbf{q}} \left[\int_0^{\omega-\mu} d\nu g^2(\mathbf{k}, \mathbf{q}) G_I(\mathbf{k} - \mathbf{q}, \omega - \nu) D_I(\mathbf{q}, \nu) \theta(\omega - \nu - \mu) + \int_{\omega-\mu}^0 d\nu g^2(\mathbf{k} - \mathbf{q}, -\mathbf{q}) \right. \\
&\quad \left. G_I(\mathbf{k} - \mathbf{q}, \omega - \nu) D_I(-\mathbf{q}, -\nu) \theta(\mu - \omega + \nu) \right], \quad \Pi_I(k, \omega) = \frac{1}{\pi} \left[\int_{\mu-\omega}^{\mu} d\nu \sum_{\mathbf{q}} g^2(\mathbf{q}, \mathbf{k}) G_I(\mathbf{q}, \omega + \nu) G_I(\mathbf{q} - \mathbf{k}, \nu) \right. \\
&\quad \left. \theta(\omega) + \int_{\mu}^{\mu-\omega} d\nu \sum_{\mathbf{q}} g^2(\mathbf{q}, \mathbf{k}) G_I(\mathbf{q}, \omega + \nu) G_I(\mathbf{q} - \mathbf{k}, \nu) \theta(-\omega) \right]. \tag{8}
\end{aligned}$$

The derivation of Eq. 8 involves a convolution of spectral functions utilizing the following representation for the delta function: $\delta(x) = \frac{1}{\pi} \lim_{\eta \rightarrow 0} \frac{\eta}{x^2 + \eta^2}$.

The real parts are obtained by the Kramers-Kronig relation

$$\begin{pmatrix} \Sigma_R(\mathbf{k}, \omega) \\ \Pi_R(\mathbf{k}, \omega) \end{pmatrix} = \frac{1}{\pi} P \int_{-\infty}^{\infty} \frac{d\omega'}{\omega' - \omega} \begin{pmatrix} \text{sgn}(\omega' - \mu) \Sigma_I(\mathbf{k}, \omega') \\ \text{sgn}(\omega') \Pi_I(\mathbf{k}, \omega') \end{pmatrix}. \tag{9}$$

Here, we should mention that though the calculation of the imaginary part of the self-energy avoids the infinite energy integration limits, the calculation of the real part by Kramers-Kronig relation does involve an energy integration between $(-\infty, \infty)$ (which is done numerically in the range $(-8t, 8t)$ as discussed in Sec. A). The sum over \mathbf{q} is avoided in the calculation of the real part.

Once the Green's functions are obtained we can compute the sub-lattice/staggered magnetization which is a measure of the long range antiferromagnetic magnetic order in the system. It is given by $M_S = S - \epsilon$ where S is the spin of the system and $\epsilon = \frac{1}{N} \sum_{\mathbf{k}} (\langle a_{\mathbf{k}}^\dagger a_{\mathbf{k}} \rangle + \langle b_{\mathbf{k}}^\dagger b_{\mathbf{k}} \rangle)$, the spin deviation and $a_{\mathbf{k}}^\dagger$ and $b_{\mathbf{k}}^\dagger$ the spin-deviation operators. For an undoped isotropic antiferromagnet this leads to

$$\epsilon = \frac{1}{N} \sum_{\mathbf{k}} \left(\frac{1}{\sqrt{1 - \gamma_{\mathbf{k}}^2}} - 1 \right), \tag{10}$$

where $\gamma_{\mathbf{k}} = (\cos k_x + \cos k_y)/2$. For a 2D spin-1/2 isotropic antiferromagnet its value is $\epsilon \sim 0.197$. We should mention here that the validity of the linear spin wave theory is based on the smallness of the parameter ϵ ⁴¹.

In the case of the doped system we also have $M_S = S - \epsilon$ where we find that

$$\begin{aligned}
\epsilon &= \frac{1}{N} \sum_{\mathbf{k}} [\eta_{\mathbf{k}} (\langle \alpha_{\mathbf{k}} \alpha_{\mathbf{k}}^\dagger \rangle + \langle \beta_{-\mathbf{k}} \beta_{-\mathbf{k}}^\dagger \rangle) - (\eta_{\mathbf{k}} + 1) \\
&\quad - \gamma_{\mathbf{k}} \eta_{\mathbf{k}} (\langle \alpha_{\mathbf{k}}^\dagger \beta_{-\mathbf{k}}^\dagger \rangle + \langle \beta_{-\mathbf{k}} \alpha_{\mathbf{k}} \rangle)], \tag{11}
\end{aligned}$$

$$\eta_{\mathbf{k}} = \frac{1}{\sqrt{1 - \gamma_{\mathbf{k}}^2}}. \tag{12}$$

Now, the relationship

$$\begin{aligned}
\langle \alpha_{\mathbf{k}} \alpha_{\mathbf{k}}^\dagger \rangle &= \langle \beta_{-\mathbf{k}} \beta_{-\mathbf{k}}^\dagger \rangle = i D(k, t \rightarrow 0^+) \tag{13} \\
&\tag{14}
\end{aligned}$$

leads to

$$\langle \alpha_{\mathbf{k}} \alpha_{\mathbf{k}}^\dagger \rangle = \int_{-\infty}^{\infty} C(k, \epsilon) d\epsilon, \tag{15}$$

i.e., this is the total spectral weight of the magnon spectral function.

We are not considering the off-diagonal magnons, i.e., $\langle \beta_{-\mathbf{k}} \alpha_{\mathbf{k}} \rangle = \langle \alpha_{\mathbf{k}}^\dagger \beta_{-\mathbf{k}}^\dagger \rangle = 0$. Thus, the final expression is

$$\epsilon = \frac{1}{N} \sum_{\mathbf{k}} \left[\frac{1}{\sqrt{1 - \gamma_{\mathbf{k}}^2}} \left(2 \int C(k, \omega) d\omega - 1 \right) - 1 \right]. \tag{16}$$

The technical part of the calculation is discussed in Sec. A of appendix.

III. HOLE SPECTRAL FUNCTIONS

A. Spectral functions

The hole spectral functions for various doping concentrations are shown in Fig. 2 and Fig. 3 (in all of our figures where we present spectral functions we do that for ω greater than the Fermi level) for the cases of the $t - J$ and $t - t' - t'' - J$ model respectively. The various lines in a given graph correspond to different wavevectors which are varied along the diagonal $(0, 0) \rightarrow (\pi, \pi)$ direction of the Brillouin zone with the lowest curve corresponding to $\mathbf{k} = (0, 0)$ and the middle to $\mathbf{k} = (\pi/2, \pi/2)$. There is a well-defined quasiparticle peak at $(\pi/2, \pi/2)$ which we have truncated at some finite value in order to make the other features of the spectra visible. We can see that with increasing doping the quasi-particle peak at $(\pm\pi/2, \pm\pi/2)$ gets truncated at the Fermi level (as it falls below the Fermi level upon low doping) and the higher energy string states gradually lose their strength and become broader. Fig. 2 also illustrates that for $\mathbf{k} = (0, 0)$ the lowest energy quasiparticle fades away with doping and the higher energy "string" states accumulate most of the spectral weight as the doping increases. Namely,

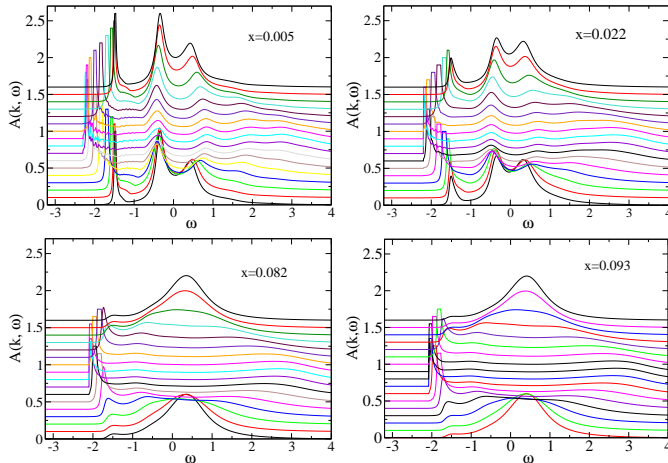


FIG. 2: Hole spectral function of the 2D $t - J$ model at $J = 0.4t (L = 32)$ for various doping concentrations x . The wavevector is varied along the diagonal $(0, 0) \rightarrow (\pi, \pi)$ direction of the Brillouin zone.

starting from the quasiparticle peak at $(\pi/2, \pi/2)$ and moving towards $(0, 0)$, we see a gradual transfer of the spectral weight from the lowest energy peak to the higher energy “string” states. This is exactly what was proposed in Ref. 12 as the origin of the waterfall-like features. Fig. 3 illustrates that a very similar behavior holds for the $t - t' - t'' - J$ model.

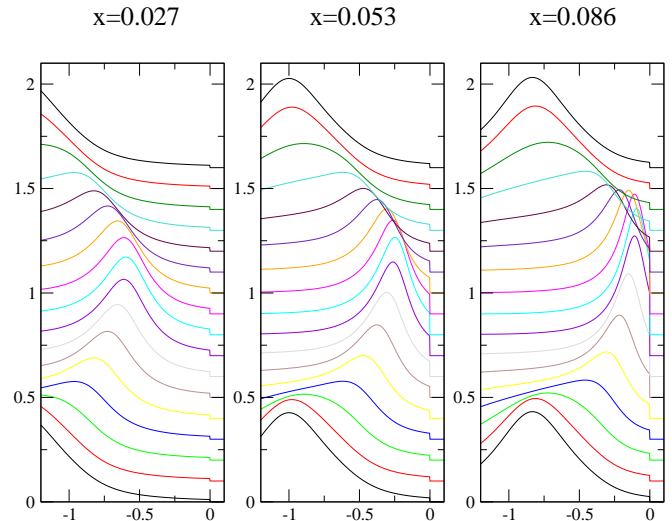


FIG. 4: Hole spectral function of the 2D $t - t' - t'' - J$ model at $J = 0.4t$ for various doping concentrations x calculated with a large value of $\eta = 0.4t$.

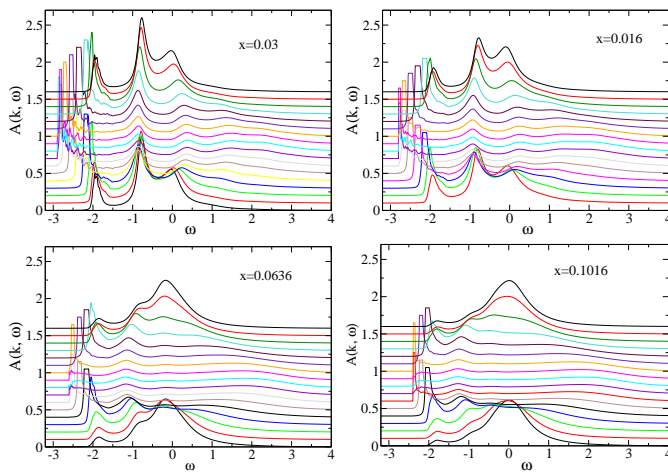


FIG. 3: Hole spectral function of the 2D $t - t' - t'' - J$ model at $J = 0.4t (L = 32)$ for various doping concentrations x . The wavevector is varied along the diagonal $(0, 0) \rightarrow (\pi, \pi)$ direction of the Brillouin zone.

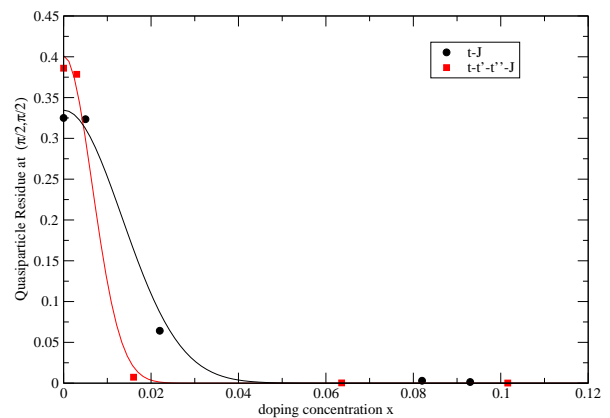


FIG. 5: Quasiparticle residue for $\mathbf{k} = (\pi/2, \pi/2)$ as a function of hole concentration for the $t - J$ and the $t - t' - t'' - J$ model at $J = 0.4t$.

Sometime ago Wells et al.¹⁴ found that there is a well-defined quasiparticle peak at $(\pi/2, \pi/2)$, within their low resolution ARPES data, which follows a dispersion with a bandwidth which is also in agreement with the results

for the $t - J$ and related models^{12,36}. Later, however, improved resolution ARPES measurements by Shen et al.¹⁵ reveal that this low energy peak is significantly broader than the limit imposed by the experimental resolution. In addition, Shen et al.¹⁵ find that the chemical potential, at low doping concentrations x , is significantly shifted from the lowest energy quasiparticle peak, thus, appearing to enter the Mott gap. Furthermore, rather recently Fournier et al.⁹ find that the quasiparticle residue is essentially zero below doping concentration of 0.1. Next we will try to understand these results within the results of our calculation. First of all, our present calculation which ignores the role of phonons shows that the lowest energy quasiparticle peak at \vec{G} is much sharper than the experimental peak. Previously¹³, we added the role of optical phonons and of finite temperature, both of which have been neglected in the present calculation, and we demonstrated that the lowest energy peak becomes broadened. In Fig. 4 we present the results of our calculation obtained using the $t - t' - t'' - J$ model for three different values of doping x and a relatively large value of the broadening parameter η , in order to compare with Fig. 3 of Ref. 15. Notice that the evolution of spectra seem qualitatively very similar to those reported in Ref. 15. In particular, we notice that the broadening causes the position of the chemical potential (the value of ω in the spectra in Fig. 4 has been shifted by the value of μ such that the position of μ is at $\omega = 0$) to move significantly away from the quasiparticle peak inside the Mott gap. This is very similar to the observation¹⁵. Therefore, we find that the results reported in Ref. 15, regarding what was referred to as “paradoxical shift” of the chemical potential, can be understood as a consequence of the broadening.

Fig. 5 illustrates the quasiparticle residue as a function of doping for the $t - J$ and the $t - t' - t'' - J$ model for $J/t = 0.4$ obtained by integrating the spectral function from $\omega = \mu$ up to the first minimum of the spectral function for $\omega > \mu$. Our results on the $t - t' - t'' - J$ model indicate that the quasiparticle residue becomes very small away from the undoped limit and as can be inferred from Fig. 4 of Ref. 9 our results are within error bars of the experimental values. In addition, Fournier et al.⁹ provide no data in the immediate vicinity of zero doping.

Therefore, we can conclude that our results can explain the ARPES^{9,14,15} results without additional hypotheses.

B. Hole energy dispersions

Fig. 6 shows a 2D contour plot of the rigid hole energy dispersion $E(k_x, k_y)$ derived from the $t - J$ model on a 32×32 lattice for $J = 0.4t$. As we follow the iso-energy lines we can see that the low energy contours are ellipses around the wave vectors $(\pm\pi/2, \pm\pi/2)$ (the lowest energies are indeed at $(\pm\pi/2, \pm\pi/2)$ which is not shown in the plot). At higher energy, the topology gradually changes and the ellipses increase in size and become con-

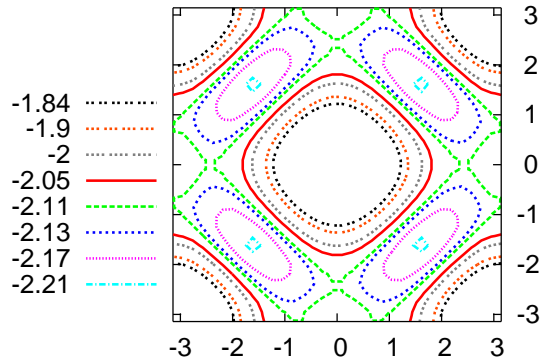


FIG. 6: Contour plots of the rigid hole energy dispersion $E(k_x, k_y)$ in the $t - J$ models for $J = 0.4t$ in a 32×32 lattice

nected to each other giving rise to new pockets around $(0, \pm\pi)$ and $(\pm\pi, 0)$. This transition occurs at doping around $x \sim 0.145$. At even higher energy these newly formed pockets disappear and disconnected contours are obtained centered around $(0, 0)$ and $(\pm\pi, \pm\pi)$ and happens above $x \sim 0.19$. A similar change of topology as function of x occurs in the $t - t' - t'' - J$ model; the main difference being that the k -space anisotropy of the spectral intensity is reduced making the hole pockets more circular than elongated.

The contour plot of the energy dispersion obtained for doped system show similar features at low doping. The hole energy dispersion $E(k_x, k_y)$ is obtained as the lowest energy peak above μ in the spectral function as a function of \mathbf{k} . Fig. 7 shows the contour plots for hole energy dispersions at various dopings. We can see that the Fermi surfaces that are small hole pockets around $(\pm\pi/2, \pm\pi/2)$ for very small doped system, gradually get elongated along anti-nodal directions as the system is doped with more and more holes.

In Fig. 8, the calculated hole spectral intensity plots at Fermi energy, for the $t - J$ model (for $x = 0.084$, top left), and for the $t - t' - t'' - J$ (for $x = 0.094$, top right) are compared with the experimental ARPES plot (bottom) for the $Na_{2-x}Ca_xCu_2O_2Cl_2$ sample with $x = 0.1$ taken from Ref. 2. The experimental intensity plot has a banana-like shape close to $(\pm\pi/2, \pm\pi/2)$ at this doping. Our numerical results show elliptical rings centered about $(\pm\pi/2, \pm\pi/2)$ stretched along off-diagonal direction for the $t - J$ model. Our calculations are restricted in the regime where there is long-range antiferromag-

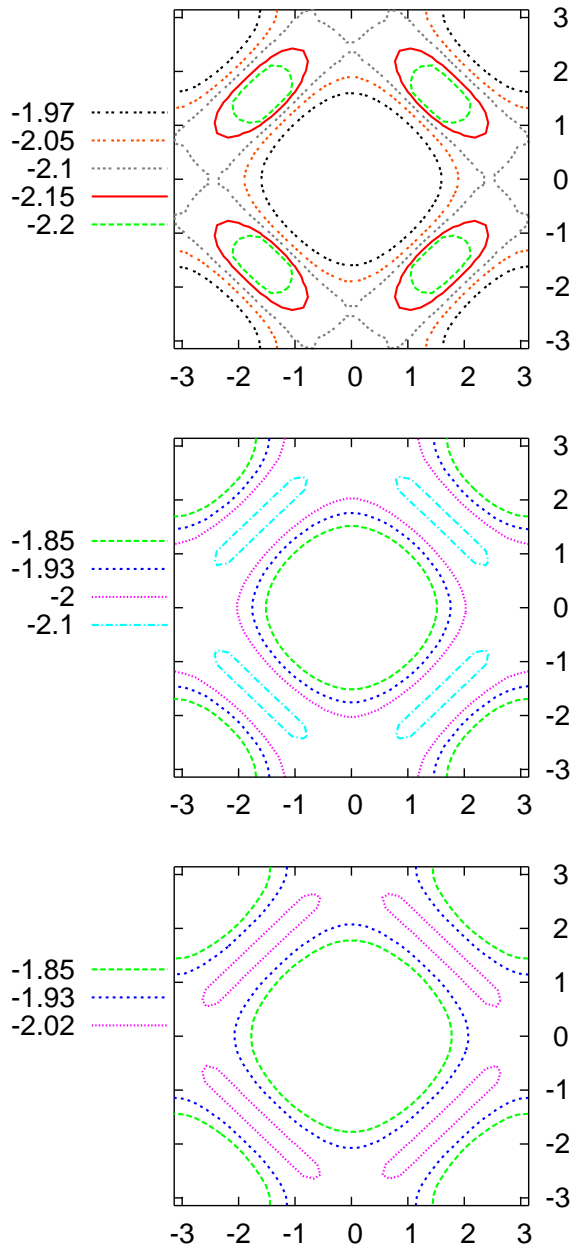


FIG. 7: Contour plots of the hole energy dispersion $E(k_x, k_y)$ for the $t - J$ model for $J = 0.4t$ in a 32×32 lattice. Top: $\mu = -2.20t$, $x = 0.022$; middle: $\mu = -2.10t$, $x = 0.082$; bottom: $\mu = -2.02t$, $x = 0.118$.

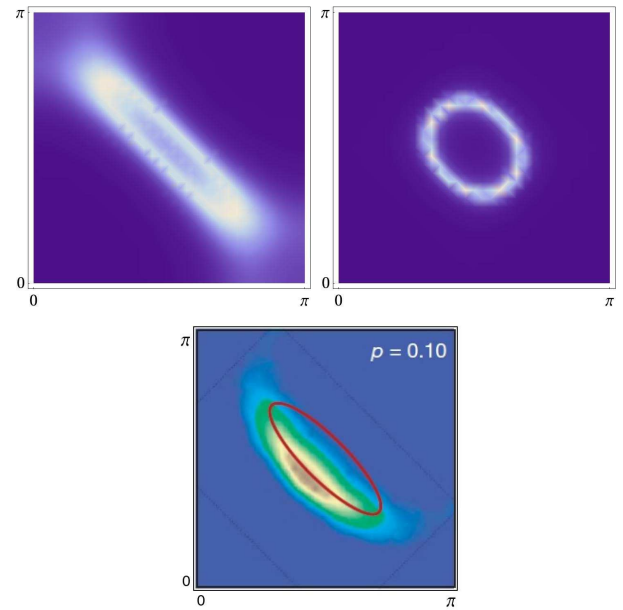


FIG. 8: Intensity plots of hole spectral functions at the Fermi energy for $J = 0.4t$ as calculated on a 64×64 lattice for the $t - J$ model (top left) at doping concentration $x = 0.084$ and for the $t - t' - t'' - J$ model (top right) at doping concentration $x = 0.094$. Bottom: ARPES intensity plot of $Na_{2-x}Ca_xCu_2O_2Cl_2$ at $x = 0.1$ done in Ref. 2 (this part of the figure is taken from Ref. 38 which was reproduced from Ref. 2 and the red elliptical Fermi arc was added). All plots show only the 1st quadrant of the Brillouin zone.

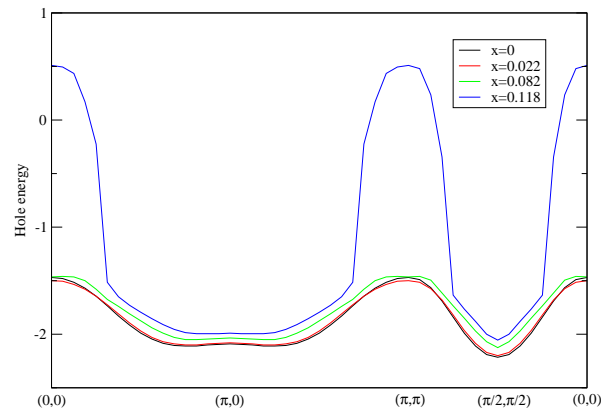


FIG. 9: Hole energy band in the $t - J$ model for $J = 0.4t$ in a 32×32 lattice along $(0, 0) \rightarrow (\pi, 0) \rightarrow (\pi, \pi) \rightarrow (\pi/2, \pi/2) \rightarrow (0, 0)$ cut in k -space.

netic order present in the system where the hole spectra should be symmetric against reflections with respect to the $(0, \pi) \rightarrow (\pi, 0)$ line in the Brillouin zone. As a result spectra having banana-like shape cannot exist in the $t - J$ or $t - t' - t'' - J$ model when there is AF order. It is possible when the long-range antiferromagnetic order is destroyed upon further doping, where the reflection symmetry with respect to the $(0, \pi) \rightarrow (\pi, 0)$ line in the Brillouin zone is broken, that the ring-like shape of the spectral intensity plot might transform to half elliptical ring-like shape which might resemble the banana shape. For example, if we cut the intensity distribution obtained for the $t - t' - t'' - J$ model shown in Fig. 8 (top right) along the $(0, \pi) \rightarrow (\pi, 0)$ line, one of the pieces will resemble the experimental intensity plot. The next nearest neighbor hoppings present in the $t - t' - t'' - J$ model reduce the k -space anisotropy of the hole pockets. However, the conclusion drawn from quantum oscillation measurements³⁸ indicate that there may be elliptical pockets centered around the $(\pm\pi/2, \pm\pi/2)$ points. These are shown by the ellipse in Fig. 8 (bottom). Therefore, it is not clear why only one side of the elliptical Fermi arcs are luminous in the ARPES studies. The ARPES result indicates that the quasiparticles are much better defined only just outside of one side of the Fermi arcs.

We should mention here that because of the finite energy resolution η in our calculation, in Fig. 8 we have also smoothed the spectral functions as follows

$$A(k, \omega) = \int A(k, \omega') \frac{\eta}{\pi((\omega - \omega')^2 + \eta^2)} d\omega' \quad (17)$$

with $\eta = 0.02t$.

Fig. 9 shows the hole bands for the $t - J$ model along $(0, 0) \rightarrow (\pi, 0) \rightarrow (\pi, \pi) \rightarrow (\pi/2, \pi/2) \rightarrow (0, 0)$ direction in k -space. The reason that a considerably larger bandwidth of the order of t is found at higher doping ($x = 0.118$) (also shown in Ref. 27) is that the lowest energy string state, as \mathbf{k} approaches $(0, 0)$ or (π, π) , loses all of its spectral weight which is transferred to higher energy string-states. However, the staggered magnetization (M_s) is zero at those doping concentrations as can be seen from Fig. 19 and so our calculation of the hole band for this value of x is outside the range of validity of our calculation.

C. Waterfall-like features

The single-hole spectral function as obtained from the $t - J$ model has high energy string states³⁶ and these states, along with the quasi-particle peak, broaden in the presence of optical phonons and finite temperature¹³. This enables a smooth transition of intensity from the low energy peak at $(\pi/2, \pi/2)$ to the high energy peak at $(0, 0)$ ¹³ as seen in the experimental waterfall-like feature⁷. Here, we find a similar fading away of the higher energy string states with doping and that makes a bridge between the high energy and low energy states so that

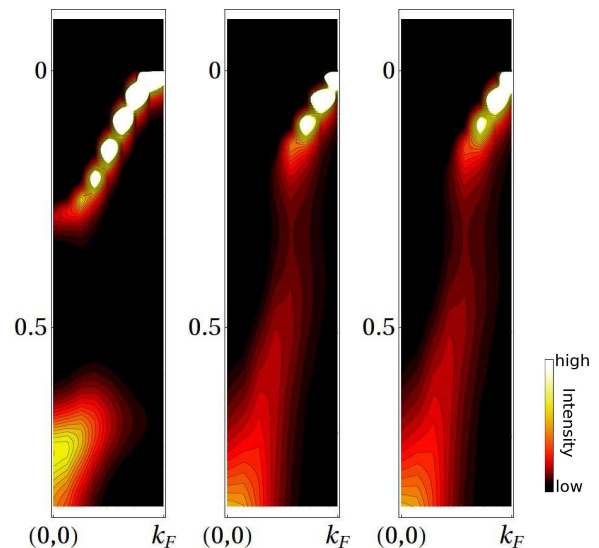


FIG. 10: Intensity plots in a 32×32 lattice from a 2D $t - J$ model for doping concentration $x = 0.02$ (left) and $x = 0.09$ (middle, right) for $J = 0.4t$. Lorentzian broadening with $\eta = 0.03t$ is used in plot at right.

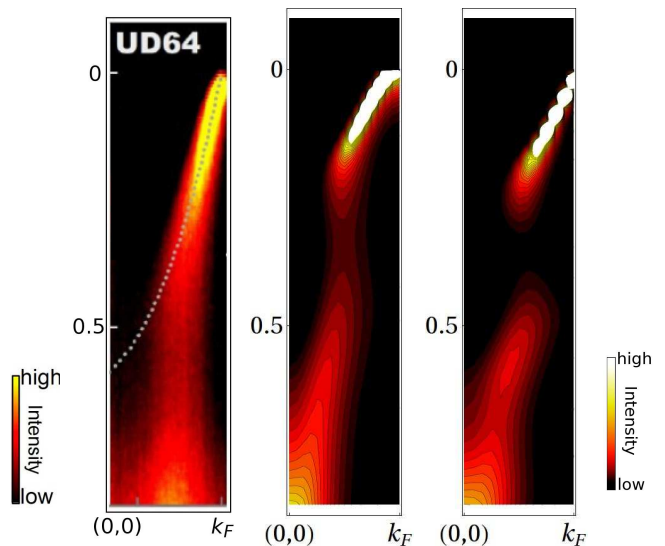


FIG. 11: Waterfall feature: ARPES intensity plot³ of underdoped Bi2212 (left) and intensity plots in a 64×64 lattice from a 2D $t - J$ model for doping concentration $x = 0.084$ (middle) and from a $t - t' - t'' - J$ model for $x = 0.094$ (right) for $J = 0.4t$.

the continuous change in the intensity gives rise to a waterfall-like pattern.

The spectral functions are smoothed as discussed by means of Eq. 17 to smooth out the “sharp edges” produced by the combination of the finite-size system and the finiteness of the energy resolution used in the numerical calculations.

Fig. 10 shows intensity plots along the nodal direction obtained using the $t - J$ model for $x = 0$ and $x = 0.09$. The discreteness of the high intensity close to Fermi wave-vector k_F is due to finite size effects and can be smoothed out when using higher values of η . Fig. 11 compares intensity plots obtained from the $t - J$ and the $t - t' - t'' - J$ model for a 64×64 size lattice with the ARPES waterfall-like intensity plots on the underdoped Bi2212. Notice a smooth transfer of intensity in the $t - J$ model intensity plots resembling the experimental ARPES plot³.

IV. MAGNETIC ORDER

A. Magnon spectral functions

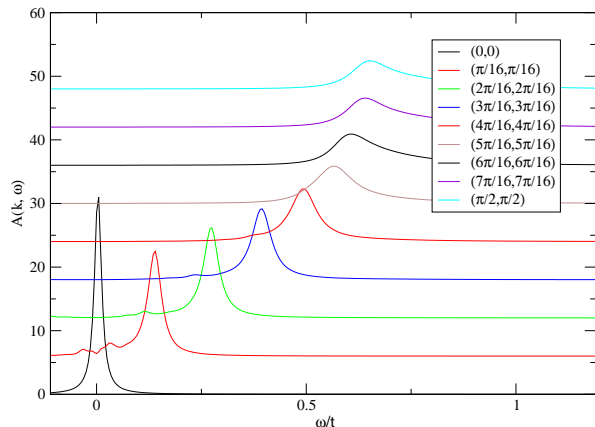


FIG. 12: Magnon spectral functions for along the diagonal of the Brillouin zone obtained for the $t - J$ model for $J = 0.4t$ ($L=32$) for $x = 0.022$.

In Fig. 12 and Fig. 13 we present the magnon spectral function for $x = 0.022$ (for a 32×32 size lattice) of the $t - J$ model along the diagonal and the $(1, 0)$ directions of the Brillouin zones respectively. For both the undoped and doped system, $D(k, \omega)$ has a rather featureless peak at the renormalized magnon energy $\Omega_r(k)$ with a width of similar order of magnitude to $\Omega_r(k)$ which is of order J , unlike the hole spectral function, which has a spread from approximately $-4t$ to $5t$ in energy. The renormalized magnon energy decreases rapidly with increased doping and at some low value of doping concentration x the spin wave spectrum collapses at small wave-vectors and this signals that the AF-LRO disappears (see also Ref. 39).

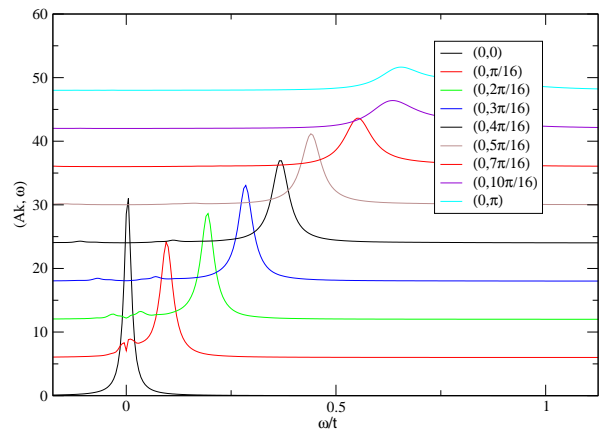


FIG. 13: Magnon spectral functions for along the $(0, 1)$ direction of the Brillouin zone obtained for the $t - J$ model for $J = 0.4t$ ($L=32$) for $x = 0.022$.

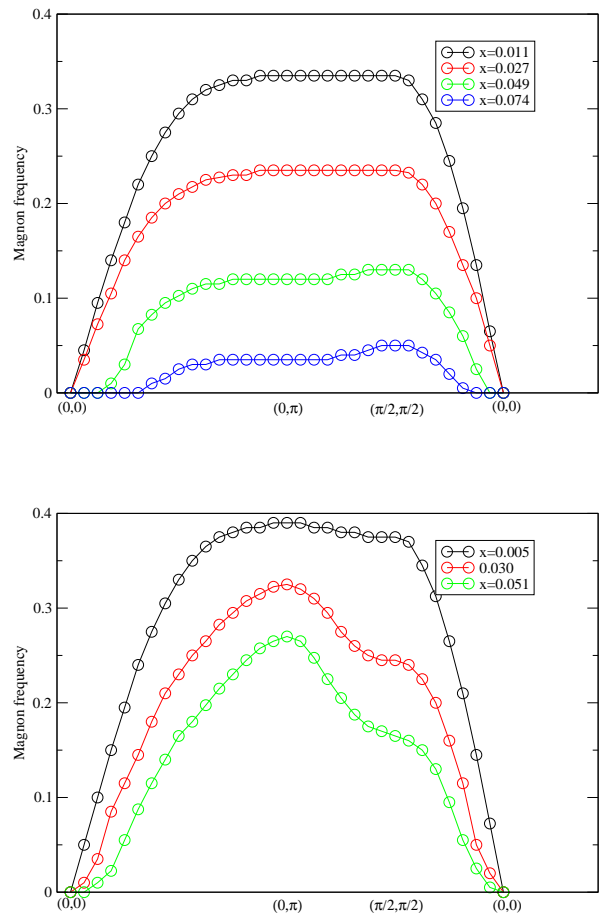


FIG. 14: Magnon frequency in the $t - J$ (top) and $t - t' - t'' - J$ (bottom) models for $J = 0.2t$.

Fig. 14 shows the spin wave dispersion as a function of doping obtained from the $t - J$ and $t - t' - t'' - J$ models in a 32×32 lattice. Doping lowers the magnon frequency and above a certain value of x it becomes zero starting at low wave-vectors.

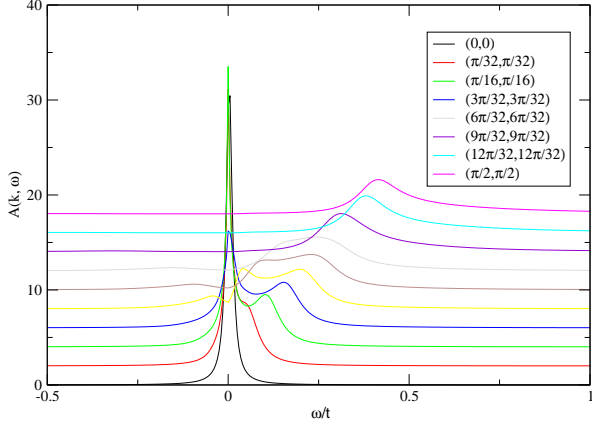


FIG. 15: Magnon spectral functions for along the diagonal of the Brillouin zone obtained for the $t - J$ model for $J = 0.4t$ ($L=64$) for $x = 0.084$.

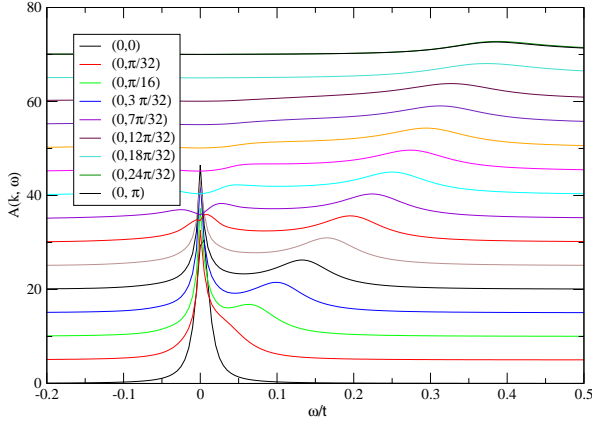


FIG. 16: Magnon spectral functions for along the $(0, 1)$ direction of the Brillouin zone obtained for the $t - J$ model for $J = 0.4t$ ($L=64$) for $x = 0.084$.

Fig. 15 and Fig. 16 shows the magnon spectral function for $x = 0.084$ (for a 64×64 size lattice) of the $t - J$ model along the diagonal and the $(1, 0)$ directions of the Brillouin zones respectively. Notice that in this case however, along with the broad magnon peak at the renormalized magnon frequency there is a sharp peak at $\omega = 0$ for small wavevectors. This is an indication of an instability which was also found by Krier et al.⁴⁰. This instability could be due to the spiral order^{28,29,34} or due to stripe ordering³⁰.

B. Staggered magnetization

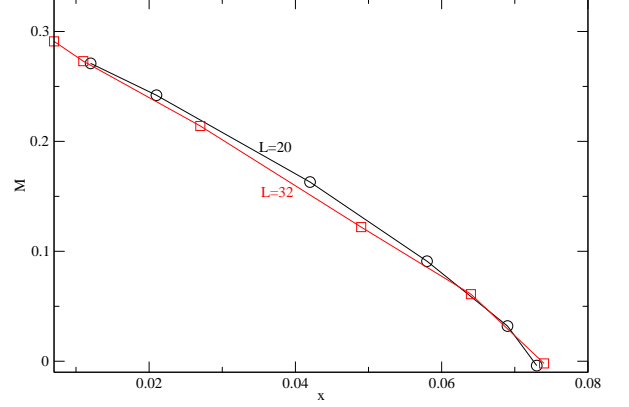


FIG. 17: Staggered Magnetization in the $t - J$ model for $L=20$ and 32 ($J = 0.2t$).

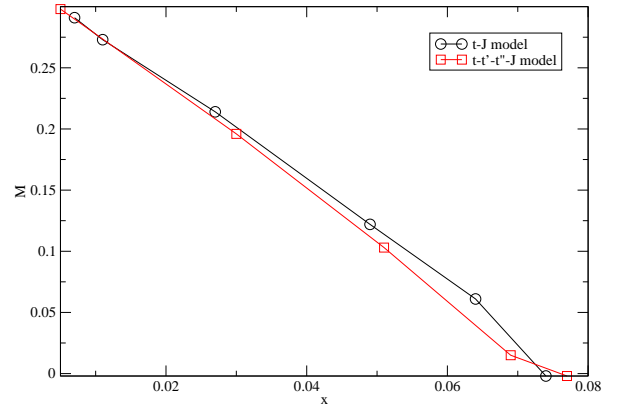


FIG. 18: Staggered Magnetization in the $t - J$ and $t - t' - t'' - J$ models for $J = 0.2t$ ($L=32$).

The staggered magnetization (M_S) for a spin-1/2 2D antiferromagnetic square lattice is 0.303^{41} . With hole doping, M_S decreases from the above value. Fig. 17 indicates that the role of finite-size effects may be insignificant. We find that M_S decreases steadily with doping and eventually goes to zero within a doping range between 0.07 and 0.08 for the value of $J = 0.2t$ (as seen in Fig. 17 and 18). Using larger values of J increases the value of the critical doping (x_c) where M_S ceases to exist. Fig. 19 shows that for $J = 0.4t$ the magnetization goes to zero at a concentration $x_c \sim 0.12$. Our staggered magnetization plots are similar to that obtained in Ref. 21–25. Following the discussion regarding the possible instabilities of our previous section, we would

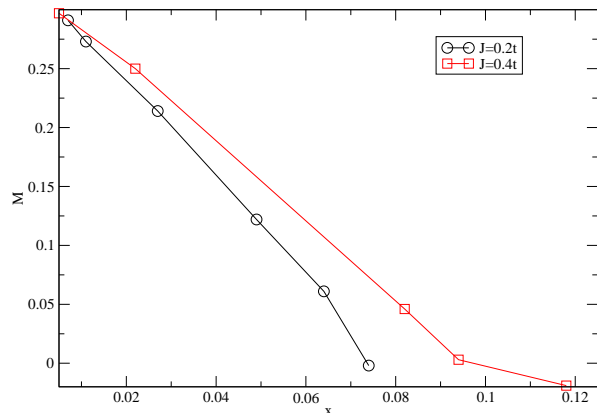


FIG. 19: Staggered Magnetization in the $t - J$ model for $J = 0.2t$ and $0.4t$ ($L=32$).

like to comment that our calculation cannot definitely distinguish the case where the antiferromagnetic order disappears due to the presence of the stripe or spiral or phase separation instabilities³³ at any doping from the case where the order disappears at a finite concentration. However, the fact that the staggered magnetization feels weak finite-size effects is an indication of the latter scenario.

V. CONCLUSIONS

We have studied the 2D $t - J$ model and the related $t - t' - t'' - J$ model in the low doping regime where the antiferromagnetic LRO is present. Our approach requires the existence of AF-LRO in order to be qualitatively correct because it starts by transforming these Hamiltonians by keeping up to quadratic terms of operators which create spin-deviations above the Néel state. We find that doping quickly reduces the degree of magnetic order and completely destroys it for doping concentration greater than $x \sim 0.08 - 0.1$ (for $0.2 \leq J/t \leq 0.4$). Experimental findings on cuprate superconductors also show quick disappearance of long range magnetic order with doping¹⁸ and when the LRO is destroyed by doping the correlation length is several lattice constants.

We find that the residue of the quasiparticle peak at $(\pm\pi/2, \pm\pi/2)$ dies out quickly with doping and in particular in the $t - t' - t'' - J$ model it becomes negligible away from the undoped limit. In addition, we find that when we broaden the lowest energy quasiparticle peak, the spectral function shares most of its features with those obtained by high resolution ARPES studies¹⁵. In particular, we find that what is called in Ref. 15 “paradoxical shift” of the chemical potential within the Mott gap, is a natural result of the broadening of the lowest energy quasiparticle peak. Our results indicate that the high resolution ARPES results obtained by Shen et al.¹⁵

and those recently reported by Fournier et al⁹ in the low doping regime can be understood in a rather simple way.

Furthermore, we studied the dependence on hole doping of the hole pockets which start forming at $(\pm\pi/2, \pm\pi/2)$ at very low hole doping when antiferromagnetic order is present in the system. We find that as we increase doping the Fermi “surface” starts as four ellipses around the wave vectors $(\pm\pi/2, \pm\pi/2)$ and the topology gradually changes where the ellipses increase in size and become connected to each other giving rise to new pockets around $(0, \pm\pi)$ and $(\pm\pi, 0)$. At even somewhat higher doping these newly formed pockets disappear and disconnected parts of the Fermi surface are obtained centered around $(0,0)$ and $(\pm\pi, \pm\pi)$. A similar change of topology as function of x occurs in the $t - t' - t'' - J$ model, the main difference being that the k -space anisotropy of the spectral intensity is reduced making the hole pockets more circular than elongated. Similar pockets have been inferred from quantum oscillation measurements³⁸ at relatively low doping.

We also find that the intensity plot of the spectral intensity has features with a ring-like shape which are centered around the wave vectors $(\pm\pi/2, \pm\pi/2)$. Our calculations are restricted in the regime where there is long-range antiferromagnetic order present in the system where the hole spectra should be symmetric against reflections with respect to the $(0, \pi) \rightarrow (\pi, 0)$ line in the Brillouin zone. As a result spectra having banana-like shape as seen experimentally², cannot exist within the models studied here when there is AF order. We argued, however, that it is possible when the long-range antiferromagnetic order is destroyed upon further doping that these features with the ring-like shape of the spectral intensity plot could transform to a half ring-like shape (i.e., a ring centered at $(\pi/2, \pi/2)$ which is scissored along the $(0, \pi) \rightarrow (\pi, 0)$ line) which might resemble the banana shape pockets near $(\pi/2, \pi/2)$ seen in the experiment².

We have also examined the role of doping in producing the waterfall-like features in the spectral function as seen in ARPES. In particular, it was suggested in Ref. 12 that these waterfall-like features is the result of spectral weight transfer from the lowest energy quasiparticle peak to the higher “string” states as the momentum varies from $(\pi/2, \pi/2)$ to $(0,0)$ along the diagonal of the Brillouin zone. We find that doping significantly broadens the high energy “string” states and this allows a gradual and continuous flow of spectral weight from the quasiparticle peak at $(\frac{\pi}{2}, \frac{\pi}{2})$ to the high energy peak at $(0,0)$. We also find that doping does not broaden the lowest energy peak enough to have agreement with the experimental waterfall-like feature, thus, other hole decay mechanisms such as decay into phonons or broadening due to finite temperature¹³ may be needed.

VI. ACKNOWLEDGMENTS

We wish to thank A. Damascelli for useful discussions.

Appendix A: Technical part

For the numerical calculation, we always keep the energy resolution, i.e., the finite-frequency step $\Delta\omega$ ($0.005t$) less than η (we used η between $0.4t$ and $0.01t$) so that the Lorentzian feature of the bare Green's functions can be represented properly as also discussed in Refs. 13,36. The energy range between which we iterate both the Green's functions are $(-8t, 8t)$ as the variance of the spectra are always well within such limit. We should mention here that the $\Delta\omega$ used in Ref. 27 that gives 400 equally spaced points in the range $-5t$ to $4t$ is larger than the Lorentzian broadening, $\eta = 0.015t$ that they used.

We find that the convergence of the self-consistent equations is slow for the doped antiferromagnet (compared to the calculations done in Ref. 36 for obtaining the hole Green's functions from undoped system). Compared to the $t-t'-t''-J$ model the convergence is even slower for the $t-J$ model as they have a complete degeneracy in the bare hole energy. In order to obtain a quick convergence we update the spectral functions, in each iteration step, by mixing the values obtained from the last two iterations- a technique also adopted in Ref. 42. We also notice poor convergence of self-consistent equations as M_S becomes very small.

When calculating the staggered magnetization, we use $C_1(k, \omega) = -D_I^{(11)}(k, \omega)/\pi$ for both positive and negative ω . Numerically a Lorentzian of width η is used to describe the imaginary part of the bare Green's function $D_0^{(11)}$, which actually should be a delta function at the non-negative energy Ω_k . And, thus, to obtain the normalization correctly, we also need to consider the tail of the Lorentzian even though that extends to negative ω .

We note that in calculating the imaginary part of the hole self-energy, the energy convolution is utilized to get rid of the infinite integration limits. However in that derivation the Lorentzian approximation of the delta function overlooks the finite Lorentzian-width coming from the finite η .

We find that the density of states below the quasi-particle peak, as obtained from the numerical calculation, depends strongly on the value of the broadening parameter, η used. This is an error which comes as a result of the finite η used in numerical calculations but this η -dependence reduces significantly as higher values of Fermi energy (i.e., higher doping concentrations) are considered. Table I illustrates the result for $J = 0.4t$ on a $t-J$ model rigid band. The numerical results coming from a system where the Fermi level stays much higher than the quasi-particle energy has a smaller error due to finiteness of the η -used. While studying the hole energy bands from the doped system we have, thus, considered only the cases where the Fermi energy is higher than the quasi-particle peak position (which is at $\sim -2.21t$ for $J = 0.4t$).

The density of states (DOS) at low energies (close to Fermi energy of the undoped system) becomes modified

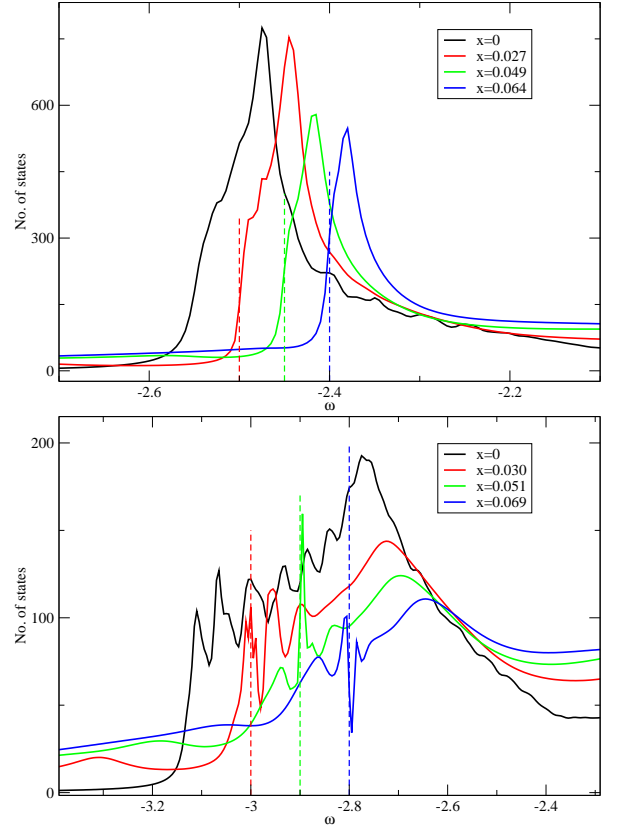


FIG. 20: Hole density of states (number of states in each of our $\delta\omega$) in the $t-J$ (top) and $t-t'-t''-J$ (bottom) models for $J = 0.2t$ ($L=32$). The positions of μ are also shown.

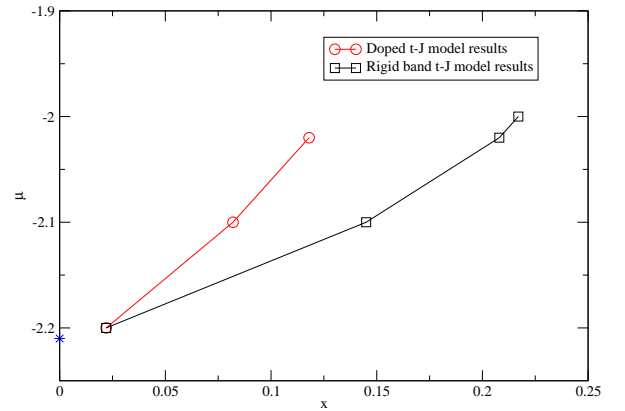


FIG. 21: Variation of μ with doping concentration x for $J = 0.4t$ in a 32×32 lattice. The blue star on the y-axis at energy $-2.21t$ shows the quasi-particle peak position of the undoped antiferromagnet.

TABLE I: Doping concentrations at different μ for different sets of η

$\eta \backslash \mu$	-2.7	-2.5	-2.4	-2.3	-2.2	-2.1	-2.0
0.1	0.0028	0.0041	0.0053	0.0080	0.0269	0.142	0.216
0.01	0.0019	0.0027	0.0034	0.0053	0.0218	0.145	0.217

with doping (Fig. 20) and the DOS low energy peaks move towards higher values at higher dopings (also see Ref. 27). This shifting of the low energy states towards higher energies causes the chemical potential to change rapidly with doping as compared to that calculated on a single hole rigid band as shown in Fig. 21. In the range of doping in which we are able to study the doped system within the realm of the LSW approximation we do not see μ to cross the DOS low energy peak for the $t - J$ model. In the $t - t' - t'' - J$ model, on the other hand, the low energy peaks in the DOS are much flatter and μ is seen to cross a few of them even at low doping (Fig. 20).

As was discussed in the introduction our results differ significantly from those of Ref. 27. For example, we find that the staggered magnetization decreases very rapidly with doping becoming zero for $x \sim 0.08$ (at $J/t = 0.2$). In contrast, in Ref. 27 results were presented for much larger values of doping concentration x (~ 0.25), where accord-

ing to our calculation, this type of calculation, which requires presence of antiferromagnetic long-range order, is invalid. The dependence of our magnon spectra with doping is also consistent with the vanishing of the staggered magnetization at $x \sim 0.08$. Namely, the renormalized magnon energy softens with doping, for small k values, becoming practically zero for $x \sim 0.08$ (for $J = 0.2t$).

Because of the above disagreement we subjected our code to several tests. We calculated the self-energies for a single iteration using our program and the result agrees with the results which we obtain using the mathematical expressions obtained analytically. Second our results for the spectra at very small doping matches well with the single hole spectra (as computed in Ref. 36) at energies higher than the quasi-particle peak of the undoped antiferromagnet. We also check the dependence of energy resolution ($\Delta\omega$) on our numerical integration ($I_{\Delta\omega}$) and find that $I - I_{\Delta\omega} \sim (\Delta\omega)^2$, as it should be.

-
- ¹ A. Damascelli et al., Rev. Mod. Phys. **75**, 473 (2003).
² K. Shen, et al., Science **307**, 901 (2005).
³ J. Graf et al., Phys. Rev. Lett. **98**, 067004 (2007).
⁴ D. S. Inosov et al., Phys. Rev. Lett. **99**, 237002 (2007).
⁵ B.P. Xie, et al., Phys. Rev. Lett., **98**, 147001 (2008).
⁶ T. Valla et al., Phys. Rev. Lett. **98**, 167003 (2008).
⁷ M. A. Hussain et al., Nature Physics **4**, 527 (2008).
⁸ X. Zhou et al., Phys. Stat. Solidi A **209**, No. 12, 2674 (2010).
⁹ D. Fournier et al., Nature Physics **6**, 905 (2010).
¹⁰ S. Basak et al., Phys. Rev. B **80**, 214520 (2009).
¹¹ A. Macridin, M. Jarrell, T. Maier and D. J. Scalapino, Phys. Rev. Lett. **99**, 237001 (2007).
¹² E. Manousakis, Phys. Rev. B **75**, 035106 (2007); E. Manousakis, Phys. Lett. A **362**, 86 (2007).
¹³ S. Kar, E. Manousakis, Phys. Rev. B **78**, 064508 (2008).
¹⁴ B. O. Wells, et al., Phys. Rev. Lett. **74**, 964 (1995).
¹⁵ K. M. Shen, et al., Phys. Rev. Lett. **93**, 267001(2004).
¹⁶ J. Igarashi, P. Fulde, Phys. Rev. B **45**, 12357 (1992).
¹⁷ I. R. Pimentel, F. C. Dias, L. M. Martelo, R. Orbach, Phys. Rev. B **60**, 12329 (1999).
¹⁸ B. Keimer et al., Phys. Rev. B **46**, 14034 (1992).
¹⁹ T. E. Mason et al., Phys. Rev. Lett. **68**, 1414 (1991).
²⁰ B. Kyung et al., Phys. Rev. B **55**, 3886 (1997).
²¹ M. Kircan, M. Vojta, Phys. Rev. B **73**, 014516 (2006).
²² G. Khaliullin, P. Horsch, Phys. Rev. B **47**, 463 (1992).
²³ J. Gan, F. Mila, Phys. Rev. B **44**, 12624 (1991).
²⁴ F. C. Dias, I. R. Pimentel, R. Orbach, Phys. Rev. B **61**, 1371 (2000).
²⁵ A. Belkasri, J. L. Richard, Phys. Rev. B **50**, 12896 (1994).
²⁶ B. Kyung, S. I. Mukhin, Phys. Rev. B **55**, 3886 (1996).
²⁷ A. Sherman, M. Schreiber, Phys. Rev. B **50**, 12287 (1994).
²⁸ C. Jayaprakash, H. R. Krishnamurthy, and S. Sarker, Phys. Rev. B **40**, 2610 (1989).
²⁹ B. I. Shraiman and E. D. Siggia, Phys. Rev. Lett. **61**, 467 (1988); **62**, 1564 (1990).
³⁰ S. White and D. J. Scalapino, Phys. Rev. Lett., **80**, 1272 (1998); **81**, 3227 (1998).
³¹ C. S. Hellberg, and E. Manousakis, Phys. Rev. Lett., **83**, 132 (1999).
³² V. J. Emery, S. A. Kivelson, and H. Q. Lin, Phys. Rev. Lett. **64**, 475 (1990).
³³ C. S. Hellberg and E. Manousakis, Phys. Rev. Lett. **78**, 4609 (1997).
³⁴ D. Yoshioka, J. Phys. Soc. Jpn. **58**, 1516 (1991).
³⁵ F. Ronning et al., Phys. Rev. B **71**, 094518 (2005).
³⁶ Z. Liu, E. Manousakis, Phys. Rev. B **45**, 2425(1992); *ibid* Phys. Rev. B **44**, 2414 (1991). See also references therein.
³⁷ Z. Liu, E. Manousakis, Phys. Rev. B **51**, 3156(1995).
³⁸ N. Doiron-Leyraud et al., Nature **447**, 565 (2007).
³⁹ D. Y. Kei Ko, Phys. Rev. Lett. **65**, 116 (1990).
⁴⁰ G. Krier, G. Meissner, Ann. Physik **505**, 738 (1993).
⁴¹ E. Manousakis, Rev. Mod. Phys. **63**, 1 (1991).
⁴² A. Sherman, Phys. Rev. B **55**, 582 (1997).